AD-A093 845 TEXAS UNIV AT AUSTIN DEPT OF CHEMISTRY F/G 9/1
SEMICONDUCTOR ELECTRODES. XXXIII. PHOTOELECTROCHEMISTRY OF N-TY--ETC(U)
JAN 81 H S WHITE, F F FAN, A J BARD N00014-78-C-0592

UNCLASSIFIED NL

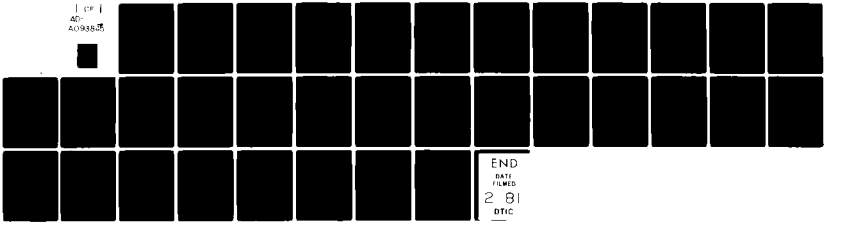

OFFICE OF NAVAL RESEARCH

Contract N00014-78-C-0592

Task No. NR 051-693

TECHNICAL REPORT No. 12

Semiconductor Electrodes XXXIII. Photoelectrochemistry of n-Type WSe_2 in Acetonitrile

by

Henry S. White, Fu-Ren F. Fan and Allen J. Bard

Prepared for Publication

in the

Journal of the Electrochemical Society

The University of Texas at Austin
Department of Chemistry
Austin, Texas 78712

January 6, 1981

SECURITY CLASSIFICATION OF THIS PAGE (When Data Entered)

REPORT DOCUMENTATION PAGE

READ INSTRUCTIONS BEFORE COMPLETING FORM

1. REPORT NUMBER: 12	2. GOVT ACCESSION NO.: AD-A093845
3. RECIPIENT'S CATALOG NUMBER: Technical rept. no 12	
4. TITLE (and Subtitle): SEMICONDUCTOR ELECTRODES. XXXIII. PHOTOELECTROCHEMISTRY IN n-TYPE WSe_2 IN ACETONITRILE.	5. TYPE OF REPORT & PERIOD COVERED: 1 Sep 80 - 31 Aug 81
	6. PERFORMING ORG. REPORT NUMBER
7. AUTHOR(s): HENRY S. WHITE, FU-REN F. FAN, ALLEN J. BARD	8. CONTRACT OR GRANT NUMBER(s): N00014-78-C-0592
9. PERFORMING ORGANIZATION NAME AND ADDRESS: Department of Chemistry, University of Texas at Austin, Austin, TX 78712	10. PROGRAM ELEMENT, PROJECT, TASK AREA & WORK UNIT NUMBERS
11. CONTROLLING OFFICE NAME AND ADDRESS: Office of Naval Research, 800 N. Quincy, Arlington, VA 22217	12. REPORT DATE: January 6, 1981
	13. NUMBER OF PAGES: 34
14. MONITORING AGENCY NAME & ADDRESS (if different from Controlling Office)	15. SECURITY CLASS. (of this report): Unclassified
	15a. DECLASSIFICATION/DOWNGRADING SCHEDULE

16. DISTRIBUTION STATEMENT (of this Report)

This document has been approved for public release and sale;

its distribution is unlimited.

17. DISTRIBUTION STATEMENT (of the abstract entered in Block 20, if different from Report)

18. SUPPLEMENTARY NOTES

Prepared for publication in the Journal of the Electrochemical Society

19. KEY WORDS (Continue on reverse side if necessary and identify by block number)

semiconductor
photoelectrochemistry
photovoltaic

20. ABSTRACT (Continue on reverse side if necessary and identify by block number)

The photoelectrochemical behavior of n-type WSe_2 single crystal electrodes in acetonitrile solutions containing several redox couples (I^-/I_3^-, Br^-/Br_3^-, Cl^-/Cl_3^-, thianthrene$^{0/+}$, $Ru(bpy)_3^{2+/3+}$) was investigated. Electrodes with discontinuities in the van der Waal's surface show large dark currents and recombination of electrons with photooxidized solution species. Pretreatment of such a surface with Cl^- passivates these dark active sites and increases the photocurrent density. The observed photopotentials at WSe_2 for redox couples with potentials, V_{redox}, more positive than 0.5 V vs. SCE show behavior consist-

DD FORM 1 JAN 73 1473 EDITION OF 1 NOV 65 IS OBSOLETE
S/N 0102-014-6601 |

Unclassified
SECURITY CLASSIFICATION OF THIS PAGE (When Data Entered)

347830

ent with Fermi level pinning; the onset potential of photocurrents increases linearly with increasing V_{redox} while the photopotential remains constant. The energy position at which pinning occurs depends on the density of surface states and the concentration of solution species. The characteristics of a photovoltaic cell based on the n-WSe_2/Cl^-, Cl_2/Pt system is also described.

Semiconductor Electrodes XXXIII.

Photoelectrochemistry of n-Type WSe_2 in Acetonitrile

Henry S. White, Fu-Ren F. Fan, and Allen J. Bard

Department of Chemistry

The University of Texas at Austin

Austin, Texas 78712

(ABSTRACT)

The photoelectrochemical behavior of n-type WSe_2 single crystal electrodes in acetonitrile solutions containing several redox couples (I^-/I_3^-, Br^-/Br_3^-, Cl^-/Cl_3^-, thianthrene$^{0/+}$, $Ru(bpy)_3^{2+/3+}$) was investigated. Electrodes with discontinuities in the van der Waals' surface show large dark currents and recombination of electrons with photooxidized solution species. Pretreatment of such a surface with $Cl^-_{(g)}$ passivates these dark active sites and increases the photocurrent density. The observed photopotentials at WSe_2 for redox couples with potentials, V_{redox}, more positive than 0.5 V vs SCE show behavior consistent with Fermi level pinning; the onset potential of photocurrents increases linearly with increasing V_{redox} while the photopotential remains constant. The energy position at which pinning occurs depends on the density of surface states and the concentration of solution species. The characteristics of a photovoltaic cell based on the n-WSe_2/Cl^-, Cl_2^-/Pt system is also described.

(End of abstract)

INTRODUCTION

The performance of photoelectrochemical devices for conversion of solar to chemical and electrical energy can be critically limited by processes occurring via intermediate energy levels at the semiconductor/liquid interface (surface states). Surface recombination and Fermi level pinning are two such processes that generally are detrimental to efficient energy conversion. In either case the photoelectrochemical results are somewhat different from expectations based on the idealized model (1) of the semiconductor electrode/solution interface. A number of investigations of the dependence of potential distribution (2) and charge transfer kinetics (3) on surface states have been carried out. The surface pretreatment or modification procedures can influence the distribution and density of surface states at energies located within the band-gap and thus cause changes in the electrochemical behavior (4,5).

Recently, Tributsch and co-workers have introduced photoelectrochemical cells based on layer-type transition metal dichalcogenides (5). These and later investigations (6-11) have shown that the observed photopotentials in aqueous (5f,9) and nonaqueous (6-8) solutions are smaller than the expectations based on the ideal junction model. Lewerenz (10), Tributsch (11) and co-workers have also recently investigated the role of surface morphology on conversion efficiencies of layered semiconductors in aqueous solutions. We report here an investigation of n-type WSe_2 electrodes in acetonitrile (MeCN) solutions. The effect of the nature of the surface and pretreatment procedures on the electrochemical response and a photovoltaic cell based on the photogeneration of chlorine at n-type WSe_2 immersed in a MeCN solution containing Cl^-/Cl_2 is described.

EXPERIMENTAL

Semiconductor Electrodes

N-type WSe_2 single crystals were generously donated by Drs. Barry Miller and Frank DiSalvo of Bell Laboratories. Electrical contacts were made to the back of each crystal by rubbing In/Ga alloy into the crystal to which a copper lead was contacted with silver epoxy cement (Allied Products Corp, New Haven, Conn.). A clean new crystal face ($\perp$C axis) was exposed by sticking adhesive tape on the front side and gently pulling off the top surface layer. To obtain electrodes with only the van der Waal's surface ($\perp$ C axis) exposed, a very minute surface area was carefully chosen that was free from any edges or face defects; these are known to provide recombination centers (10, 11). Such electrodes are designated "Type S" in this paper. No electrodes were prepared with only the surface $\parallel$ C axis exposed, since the crystals were only $\sim$ 1-2 mm thick along this plane and are difficult to mount without leaking. Electrodes were prepared from several crystals that had visible edges (discontinuities in the otherwise smooth van der Waal's plane) exposed to the solution. These electrodes are designated "Type E." Scanning electron micrographs of Type S and Type E WSe_2 electrodes are shown in Fig. 1. The surface defects represented roughly 5-10 % of the total surface area of Type E electrodes.

The crystal sides and back and the copper lead were completely covered with 5-minute epoxy cement; this was then covered with silicone rubber sealent (Dow Corning Corp., Midland, Mich). For long-term stability measurements involving strong oxidants, such as Cl_2, the electrode was covered with a pre-activated photo-cure epoxy cement that is used in dental restorative work (Caulk Nuva-Fil, D.A., Milford, Del). The exposed areas of the crystal faces, in both types of electrodes were between 0.010 and 0.070 cm^2.

Unless noted otherwise, before each experiment the electrodes were etched in 12 M HCl for 15-30 sec, rinsed thoroughly with distilled water and dried under vacuum for 1 hr. The electrodes were then stored inside a He-filled dry box (Vacuum Atmospheres, Hawthorne, Cal.) and used within one day.

Chemicals

All electrochemical grade tetralkylammonium salts were purchased from Southwestern Chemical Company (Austin, TX). Tetrabutylammonium perchlorate (TBAP), tetrabutylammonium bromide (TBABr), tetramethylammonium chloride (TMACl) and tetrabutylammonium iodide (TBAI) were recrystallized at least twice from acetone-ether and dried under vacuum for two days. Tetraethylammonium chloride (TEAC) was recrystallized from MeCN-ether and dried as above. Thianthrene (Th) (Aldrich Chem.) was either sublimed three times or recrystallized from benzene twice. $Ru(bpy)_3(ClO_4)_2$ was prepared and purified as previously described (12). After purification the reagents were stored inside the dry box. I_2 (Fischer Scientific Company), Br_2 (MCB), and Cl_2 (Matheson Gas Company) were used without further purification. MeCN was purified and dried as previously described (13) and stored inside the dry box.

Electrochemical Apparatus

Voltammetric measurements were made in a two compartment cell (30 ml) equipped with an optically flat Pyrex window. The working and reference electrodes were separated from the auxilliary electrode, a Pt flag ($\sim$ 8 cm^2), by a medium-porosity frit. Along with the semiconductor electrodes the main compartment contained a Pt disk (0.025 cm^2) sealed in glass that was used to check the purity of the electrolyte and to locate the potential of the reference electrode with respect to the potential of a known reversible redox couple. The reference electrode was a polished silver wire inside a glass

cylindrical compartment containing only the supporting electrolyte and separated from the main solution by a medium porosity frit. All potentials reported here are referenced to an aqueous saturated calomel electrode (SCE). Single compartment, two electrode cells, also equipped with optically flat Pyrex windows, were used as photovoltaic (solar) cells.

The electrochemical cell and solutions were prepared before each experiment within the dry box. All ground glass joints were sealed with silicone-based vacuum grease to permit the cell to be removed from the inert atmosphere for study. When the experiment required opening of the electrochemical cell outside of the dry box, pre-purified N_2 was blown over the top of the solution until the cell was reclosed.

The cyclic voltammograms were obtained with a Princeton Applied Research (PAR) Model 173 potentiostat and PAR Model 175 Universal programmer and recorded on a Houston Instruments Model 2000 X-Y recorder. Capacitance measurements were made using a PAR Model HR-8 lock-in amplifier. Solar cell current-voltage curves were made by measuring the voltage across a variable load resistance with a Keithly Model 179 TRMS digital multimeter.

The light source used for photoelectrochemical studies was an Oriel Corp. (Stanford, Conn.) 450 W xenon lamp. A red-filter was used to eliminate wavelengths below 590 nm. Neutral density filters (Oriel Corp.) were used to vary the light intensity. The full, filtered xenon lamp power output was $\sim$ 150 mW/cm^2 as measured with an E. G. & G. (Salem, Mass.) Model 550 radiometer/photometer and a Scientech 361 power meter.

RESULTS

Capacitance measurements and cyclic voltammetry in the absence of redox couple. - Capacitance measurements on several n-WSe_2 electrodes in MeCN containing only TBAP (0.2 M) resulted in two distinct types of behavior. The

capacitance versus potential curve of a Type S electrode, Fig. 2, closely resembles behavior typical of a fairly large band-gap n-type semiconductor, where at potentials positive of the flat-band potential, V_{fb}, the space charge region is depleted of electrons and contains ionized donors at some constant concentration (1). This region extends up to potentials of 1.3 V vs. SCE. At potentials more negative than -0.4 V, the capacitance becomes constant indicating the onset of degeneracy. The voltammetric behavior of the same electrode in MeCN-0.2 M TBAP is shown in Fig. 3. In the dark a small current, $\sim$ 0.2 mA/cm^2, begins at 0.6 V. Under illumination, the photocurrent begins at $\sim$ 0.5 V and increases steadily at more positive potentials. At 1.0 V, the photocurrent is $\sim$ 1.0 mA/cm^2. On the reverse scan, under illumination, a small cathodic current, $\sim$ 0.2 mA/cm^2, begins at 0.0 V. This same cathodic current is observed if the light is turned off on the reverse scan and increases with more positive switching potentials. The anodic photocurrent and induced dark current are probably due to the oxidation and re-reduction of the crystal surface caused by traces of H_2O in the acetonitrile (5e). Further purification of the solvent by addition of Al_2O_3 significantly reduced these currents.

The capacitance behavior of a Type E WSe_2 electrode, also shown in Fig. 2, is typical of electrodes with discontinuities in the van der Waal's surface. The branch towards negative potentials is similar in shape to the Type S electrodes. However, at potentials more positive than 0.7 V, the capacitance increases sharply indicating either deep surface states, inversion of the space charge region, or the occurence of a faradaic process. As Tributsch has already pointed out (5e), inversion of the space charge region in a semiconductor with a band-gap of 1.4 eV volts is unlikely within this potential region. If space charge inversion due to thermal activation of electrons into the conduction band were responsible for this increase in capacitance, both Type S and Type E electrodes should show this behavior. The voltammetric

behavior of the same crystal (Type E) in a blank solution is shown in Fig. 3. A dark anodic current is observed that is approximately five times larger than on the Type S electrode (compare at 1.0 V). Under illumination, a photocurrent begins at -0.3 V and is fairly constant until 0.7 V where a sharp increase in anodic currents begins. The net photocurrent density at 1.0 V is $\sim$ 0.6 mA/cm^2, which is $\sim$ 60 % the current density at the Type S electrode. The V_{fb}-values and donor densities of these crystals were estimated from the capacitance measurements. Mott-Schottky plots for the two crystals described above are shown in Fig. 4a and 4b. The results for several crystals are summarized in Table 1. V_{fb}, for WSe_2 in MeCN, estimated by extrapolating to the potential where $1/C_{sc}^2 = 0$, was always in the range of -0.2 to -0.4 V vs SCE. The apparent donor densities, n_D, for Type E electrodes were 7 to 10 times larger than for Type S electrodes. As can be seen in the Mott-Schottky plots, the apparent capacitance values were highly dependent on the frequency of the applied alternating voltage. Frequency dispersion of the capacitance due to dielectric relaxation should be negligible in a covalent-type material like WSe_2. It is possible that the dispersion observed here is due to small changes in the effective electrode surface due to corrosion. The values of n_D listed in Table 1 are from measurements in the range 500-1000 Hz. A value of 10 for the dielectric constant of WSe_2 was used in all calculations (16).

Voltammetric behavior of various redox couples at n-WSe_2. - Type S and E electrodes showed distinctly different voltammetric behavior. Recall that Type E electrodes are those that have visible edges or discontinuities in the van der Waal's plane exposed to the solution. These edges have been associated with the face parallel to the main C axis ($\parallel$ C axis) (14) where empty conduction band orbitals are exposed to the solution. The results are summarized in Tables 2 and 3.

Oxidation of I^- and Br^-. - The Type S electrode shows negligible dark current in the vicinity of I^- oxidation on Pt (Fig. 5a). Upon illumination, the potential for onset of photocurrent, V_{on}, was 0.0 V and attains a saturation current at $\sim$ 0.2 V. The chopped light voltammogram clearly indicates that little back-reaction (reduction of photooxidized products) occurs beyond the onset potential. The dark current at the Type E electrode in the presence of I^- (Fig. 5b) was smaller (i.e. about one-tenth) than in the blank solution (Fig. 3). V_{on} was $\sim$ 0.07 V more negative than the V_{on} at the Type S electrode. This difference in onset potential is approximately the difference in the measured flat-band potentials for these crystals. The maximimum photocurrent densities were about the same for both Type S and Type E electrodes. However, on scan reversal, a much larger reduction peak centered at -0.07 V was found with the Type E electrode.

The oxidation of Br^- (as TBABr) on WSe_2 followed behavior similar to that found for I^- (Figs. 6a, 6b). The V_{on} for the Type E electrode was about 30 mV more negative than for the Type S electrode. A much larger difference existed, however, in the total photocurrent densities. The current density at the Type S electrode was about 4 to 5 times larger than that at Type E.

Oxidation of Cl^-. - The voltammetric behavior for the oxidation of Cl^- at the two WSe_2 electrodes are shown in Figs. 7a and 7b. At the Type S electrode, V_{on} is 0.55 V. Again, no dark current or back-reaction is seen at this electrode. The oxidation of Cl^- on the Type E electrode is strikingly different. V_{on} was 0.34 V more negative at this crystal. This difference in onset potential cannot be accounted for by the small difference in flat-band potential ($\sim$ 50 mV). The cyclic voltammogram at the Type E electrode shows a large reduction peak centered at 0.17 V in the dark on scan reversal. This peak probably corresponds to the reduction of chlorine generated in the dark on the anodic scan. Under

illumination, this reduction peak occurred a potential about 0.2 V more negative. No reverse reduction peak was observed in the dark on the Type S electrode since no dark anodic current flowed. However, under illumination, a similar cathodic current was observed at potentials more negative than 0.0 V.

Thianthrene. - The voltammetric behavior for the oxidation of thianthrene (Th) at the two WSe_2 crystals is shown in Figs. 8a and 8b. While under illumination, the onset potential and waveforms are almost identical at the two electrodes; in the dark a striking difference exists. With the Type E electrode, a large quasi-reversible peak is located at approximately the same potential as on Pt. The current density in the dark is equal to the photocurrent density. On the Type S electrode, no dark anodic current is observed. On scan reversal following an anodic scan under illumination, a cathodic peak is observed at both Type E and S electrodes.

Oxidation of thianthrene in the presence of halide. - The photooxidation of Th with small amounts of halide species (10-15 mM) added to the solution was studied to determine the effect of halide ions upon the photoelectrochemical behavior of WSe_2. The cyclic voltammograms obtained in the dark at the Type E electrode in mixed Th/halide solutions is shown in Fig. 9. The previously observed dark quasi-reversible wave due to Th oxidation and $Th^{+\cdot}$ reduction is noticeably absent in the presence of I^-, Br^-, or Cl^-. A comparison of the cyclic voltammograms under illumination of thianthrene alone and with either I^- or Br^- in solution shows little change in the peak potentials due to Th photooxidation. In the presence of Cl^-, however, these peaks, which were centered around 0.75 V vs SCE, are absent (Fig. 10), and instead, a new pair of oxidation and reduction waves centered at 0.52 V appeared. These peaks were not present in solutions containing Cl^- alone and therefore are assigned to the oxidation and reduction of Th. From these results, it appears

that Cl^- induces a 230 mV shift in V_{on} for the oxidation of thianthrene. To demonstrate that this effect results from the interaction of Cl^- with the surface discontinuities, the experiment illustrated by Fig. 11 was undertaken. A fresh Type E electrode was prepared and the dark and photooxidation of Th was observed (curves a, b). The electrode was then removed and dipped into a MeCN solution of 7.0 mM TEACl in the dark without any external electrical connection. After 30 sec, the electrode was removed, rinsed thoroughly with MeCN and placed back into the original Th-containing solution. The resulting cyclic voltammograms (curves c, d) showed an immediate decrease in the dark current and a negative shift ($\sim$ 180 mV) of the onset potential for photocurrent. The maximum photocurrent for Th oxidation increased by about 25 % following this surface treatment. This improved photocurrent-potential curve remained unchanged for at least 30 min of continuous cycling. When a similar experiment was carried out with a Type S electrode, no changes in the dark oxidation current (which was negligible) or the photocurrent was found by a Cl^- pretreatment. Note that the decrease in dark current for the Type E electrode upon treatment with Cl^- takes place without any possibility of photooxidation occurring during the exposure of the electrode to Cl^- so that the formation of a light-induced complex between the electrode and Cl^- is unlikely. The observed effect can be ascribed to interactions of the Cl^- with surface discontinuities leading to modification or passivation of these sites.

Photovoltaic cell based on $WSe_2/Cl^-, Cl_2, (MeCN)/Pt.$ - Schneemeyer and Wrighton have previously reported photovoltaic cells based on the generation of Cl_2 at illuminated MoS_2 (6) and $MoSe_2$ (7) in MeCN. Similar cells employing Type S WSe_2 photoanodes were constructed to test the efficiency and stability of this material. The i-V characteristics for several electrodes in cells

saturated with TEACl and with Cl_2 bubbled through the solution are shown in Fig. 12. The open circuit photovoltage, V_{oc}, and short circuit photocurrents, i_{sc}, for several electrodes are listed in Table 4.

At low photovoltages the photocurrents at several electrodes appear remarkably high, representing quantum efficiencies of 1 (or even more) under short-circuited conditions. A sharp drop in photocurrent ($\sim$ 30-40%) is observed with increasing load resistance in the first 100 mV of the photo i-V curve (Fig. 12). To determine if these unusually high currents are due to a photo-induced carrosion process, a WSe_2 crystal (11.5 mg) was placed in contact with a Pt electrode and immersed in a 2.0 M TEAC solution saturated with Cl_2. After 60 hours under illumination ($\sim$ 80 mW/cm^2) the crystal remained unchanged with no weight loss ($\pm$ 0.1 mg). While this experiment may not reproduce the actual conditions of a PEC cell, photo-induced corrosion does not appear to be the major cause of the high short circuit currents. Other causes for this result, such as the focusing or scattering of the incident radiation onto the very small area electrode by the surrounding glass or sealant to cause a higher effective light flux on the electrode have been considered. Probing experiments with the small beam of a He-Ne laser show that this is a small effect. At this time, the actual cause of these anomalous currents is unclear.

V_{oc} depended strongly upon the amount of Cl_2 bubbled through the solution. The highest V_{oc}-values listed for the 1.9 M Cl^- solutions (Table 5) were produced by optimizing the Cl^-/Cl_2 ratio. No attempt was made to measure exactly the amount of Cl_2 dissolved in the solution. As shown in Fig. 13, V_{oc} drops considerably as excess Cl_2 is added to the solution. In a regenerative photocell with an inert metal electrode and without an external power supply the photocurrent can be limited by either processes at the photoanode or at the metal cathode. Thus, at low concentrations of Cl_2 the photocurrent was limited by mass transfer to the platinum cathode, while at high Cl_2/Cl^- ratios, the

photovoltage was limited by the solution redox potential (as discussed below). When the photocurrent did not increase with higher concentrations of Cl^- or Cl_2, addition of Cl^- to the solution increased V_{oc}. The i_{sc}-value increased steadily with Cl^- concentration up to 1.6 M. Additional increases in Cl^- concentration had no effect upon i_{sc} or V_{oc}.

In a 1.9 M Cl^- solution, V_{oc} approached a constant maximum value at light intensities $\geq$ 30 mW/cm^2. The short-circuit photocurrent increased linearly with light intensity up to 120 mW/cm^2, where it also reached a saturation value.

Irradiation of the WSe_2 photoanode with the full output from a 450 W xenon lamp (> 590 nm and IR filtered) focused onto the electrode surface yielded the i_{sc} and V_{oc}-values listed in Table 4. Maximum power efficiencies under these conditions were estimated to be 7 to 10.5 %. No attempts were made to correct for solution absorption or reflections at the cell windows or electrode surface. However, since the same photocurrent was found at $\sim$ 80 % of this light intensity, the power efficiencies at lower intensities would be $\sim$ 2 % higher.

The stability of n-WSe_2 (Type S) against possible attack by Cl_2 generated at the surface was tested by allowing the photovoltaic cell to run for several hours (Fig. 14). After 7 hours, the short-circuit photocurrent had decreased by $\sim$ 4% from its original stable value of 146 μA. This corresponds to 3.7 coulombs of charge passed which represents an amount of charge sufficient to consume an appreciable part of the 10 mg crystal, if corrosion were occurring. The electrode surface appeared unchanged after 7 hours.

DISCUSSION

Dark and photocurrents. - The large differences in dark currents on the Type S and Type E electrode can be understood by a modified model used by Gerischer et al for dark currents on MoS_2 (14). In this model, the d-orbitals

parallel to the C-axis, in addition to forming the conduction band in the bulk material, are assumed to provide surface states at discontinuities of the Type E electrode at energies in the upper part of the band-gap (11). Facile electron transfers can take place from the electroactive species into the conduction band via these mediating d-orbitals. When the exposed surface is free from edges, the layer of Se atoms blocks overlap between the conduction band and molecular orbitals of the species. In this case, electron transfer in the dark via the conduction band is allowed only by thermal excitation or by tunneling. This model seems to fit the behavior found for the oxidation of Th at WSe_2. In the dark, a small current (< 0.2 mA/cm^2) is observed on the Type S electrodes. This dark current is no larger than the current observed for the same electrode in a solution containing only supporting electrolyte (0.2 M TBAP). At the Type E electrode, a large, mass-transfer-limited, dark current is observed for Th oxidation indicating that the current is not controlled by the number of dark oxidation sites on the crystal surface. Under illumination, both electrodes show similar voltammetric responses, with slightly higher photocurrents observed on the Type S electrode. Thus for the Type E electrode, the existence of the surface states allows Fermi level pinning and electron transfer to occur at potentials close to the standard potential of the redox couple. However, for a Type S electrode, there are much lower densities of surface states near the conduction band. Fast electron transfer reactions do not occur in the dark for couples with potentials much more positive than the flat-band potential. However, even with Type S electrodes, Fermi level pinning at the bottom part of the band gap may occur, as discussed later.

The photooxidation of halide species shows a slightly more complicated behavior. At the Type S electrode, the dark anodic current in the presence of halides is about the same as the small dark current observed in a solution

containing only supporting electrolyte. However, at the Type E electrode, the dark current in the presence of halides is much smaller than that in the blank solution. Tributsch et al have previously proposed an interaction of I^- with the surface in aqueous solutions (5f). The decrease in the dark oxidation currents on the Type E electrode on the addition of halide ions similarly suggests a strong interaction of I^-, Br^-, and Cl^- with the surface states, composed of empty d-orbitals along the exposed edges, deactivating these previously dark active sites. This is confirmed by the decrease in the dark currents for Th oxidation (and Th^+ reduction) by the addition of I^-, Br^-, or Cl^-.

The total photocurrent densities for the oxidation of Cl^- or Br^- are 3 to 5 times larger at the Type S electrode. Apparently while the dark active sites at the exposed edges are ineffective for the dark oxidation of Br^- or Cl^-, they remain rather efficient at trapping electrons and reducing photogenerated Cl_2 and Br_2. The total photocurrent density for the oxidation of I^- at the two electrodes was approximately the same.

The difference in behavior between Br^- or Cl^- and I^- probably reflects the stronger interaction of I^- with the electrode surface. The decrease in background current after treatment with halide (compare the dark currents at Type E electrode before and after addition of I^-, Br^-, Cl^-) is important, since this current is presumably caused by oxidation of the surface lattice in the presence of trace amounts of H_2O in the acetonitrile (5e). Suppression of the crystal oxidation is equivalent to stabilization of these photoanodes and may be the reason for the stability observed in the aqueous iodide (5e,9) and nonaqueous chloride (6,7) cells employing layered materials. Further experiments are necessary to demonstrate if the halide pretreatments are sufficient for long term stability.

Photopotentials. - From differential capacitance measurements, V_{fb} of n-type WSe_2 (both Type S and E) in MeCN/TBAP alone was -0.3 ± 0.1 V vs SCE (Table 2). The band-gap of these samples, determined from the action spectrum, is ∿ 1.4 eV. After correction for the difference between Fermi level and the conduction band edge, this places the edge of the valence band at ∿ 1.0 V vs SCE. This is in good agreement with the flat-band potential of p-type WSe_2, + 1.0 V vs SCE, measured in MeCN (15).

The difference in potential for oxidation at Pt and illuminated WSe_2 (i.e. the photounderpotential) vs the standard potential for several redox couples is shown in Fig. 15. The standard potentials taken for I^-, Br^-, and Cl^- are the average of the reduction and oxidation peak potentials at Pt. The V_{on} for I^- and Br^- is approximately 0.2 to 0.3 V positive of the measured flat-band potential. This positive value of V_{on} suggests recombination is occurring and this can be attributed to the band of surface states lying directly below the conduction band edge.

For couples with standard potentials more positive than 0.5 V vs SCE (Cl^-/Cl_2, Th/Th^+, $Ru(bpy)_3^{2+/3+}$) the photopotential (V^0-V_{on}) become almost constant at a value of ∿ 0.4 to 0.5 V. This limiting value can best be understood by Fermi level pinning (2a) at surface states located approximately 0.5 eV above the valence band edge. V_{on} for redox couples with V^0 more positive than 0.5 V vs SCE should increase linearly with increasing V^0. For couples with V^0 at potentials negative of the surface state level (< 0.5 V), V_{on} is constant and the photopotential should increase as V^0 becomes more positive, as seen in Fig. 15. Further evidence for the presence of surface states is the highly dependent nature of the photovoltage developed in the n-WSe_2/Cl^-,Cl_2 (MeCN)/Pt cell upon the Cl_2/Cl^- ratio (Fig. 13). Based on the ideal model of the semiconductor-solution interface (1), V_{on} should be at V_{fb} and the Pt electrode would be poised by the redox couple so that a

higher photovoltage is expected with higher Cl_2/Cl^- ratios, i.e. a higher Cl_2/Cl^- shifts the solution redox potential to more positive values while the band-edges remain unaffected. However, the experimental results do not conform to this behavior. Upon addition of Cl_2, V_{oc} actually decreases (see Fig. 13). This could be attributed to a higher surface recombination rate at the higher Cl_2 concentration.

The shift in onset potential for Th oxidation at the Type E electrode in the presence of Cl^- can also be explained by Fermi level pinning as shown in Scheme I (a). As the applied potential is biased in a positive direction, Cl_2 is initially generated and the Fermi level is pinned at the redox potential of Cl_2/Cl^- or, more likely, somewhere between the V's of the two redox couples. The result should be a more negative onset potential for thianthrene oxidation as is observed in Fig. 10. I^-/I_2 does not affect the onset potential for thianthrene oxidation, since at the potential where the Fermi level is pinned, i.e. at the standard potential of I^-/I_2, the valence band edge and the bottom surface states are well beyond the potential of $Th/Th^{\cdot+}$ (see Scheme I (b)).

CONCLUSION

The results presented here indicate that the surface morphology of WSe_2 single crystals is a critical factor in determining their performance characteristics in photoelectrochemical cells. Both the photocurrent and photovoltage are dependent upon the discontinuities in the surface plane. The application of layer-type semiconductors towards efficient solar conversion devices will depend upon the ability to passivate recombination centers located at these surface discontinuities. Halide pretreatment can improve the photoresponse for the oxidation of thianthrene. Surface pretreatments with other electron-donating species may passivate recombination to a larger degree and is under investigation. The correlation of the density of surface states

(surface discontinuities) with the observed photopotential lends support to the role of Fermi level pinning (2). Further results are required before an unambiguous relationship can be drawn between the density of surface states and the observed photopotential.

The stability and efficiency of the nonaqueous n-WSe_2/Cl^-,Cl_2/Pt photovoltaic cell confirm the original predictions of Tributsch (5a) on the performance of layered materials.

ACKNOWLEDGMENT

The assistance of Dr. Michael Schmerling in obtaining the electron micrographs is gratefully appreciated. This work was supported by the National Science Foundation, the Office of Naval Research, and by the Solar Energy Research Institute (in a cooperative project with SumX Corporation).

REFERENCES

(1) H. Gerischer, in "Physical Chemistry: An Advanced Treatise," H. Eyring, D. Henderson, and W. Jost, Editors, Vol. 9A, Academic Press, New York (1970).

(2) (a) A.J. Bard, A.B. Bocarsly, F.-R.F. Fan, E.G. Walton, and M.S. Wrighton, J. Am. Chem. Soc., 102, 3671 (1980); (b) F.-R.F. Fan and A.J. Bard, ibid., 102, 3677 (1980); (c) A.B. Bocarsly, D.C. Bookbinder, R.N. Dominey, N.S. Lewis, and M.S. Wrighton, ibid., 102, 3683 (1980).

(3) (a) R. Memming and G. Schwandt, Surface Sci., 5, 97 (1966); (b) R.A.L. Vanden Berghe, F. Cardon, and W.P. Gomes, ibid., 39, 368 (1973); (c) P. Kohl and A.J. Bard, J. Am. Chem. Soc., 99, 7531 (1977); (d) S. Frank and A.J. Bard, ibid., 97, 7427 (1975).

(4) (a) B.A. Parkinson, A. Heller, and B. Miller, J. Applied Physics, 33, 521 (1978); (b) B.A. Parkinson, A. Heller, and B. Miller, J. Electrochem. Soc., 126, 954 (1979).

(5) (a) H. Tributsch, Z. Naturforsch, 32a, 972 (1977); (b) H. Tributsch and J.C. Bennett, J. Electroanal. Chem. 81, 97 (1977); (c) H. Tributsch, Ber. Bunsenges. Phys. Chem., 81, 361 (1977); (d) H. Tributsch, ibid., 82, 169 (1978); (e) H. Tributsch, J. Electrochem. Soc., 125, 1086 (1978); (f) H. Tributsch, H. Gerischer, C. Clemen, and E. Bucher, Ber. Bunsenges. Phys. Chem., 83, 655 (1979); (g) J. Gobrecht, H. Gerischer, and H. Tributsch, J. Electrochem. Soc., 125, 2085 (1978).

(6) L.F. Schneemeyer and M.S. Wrighton, J. Am. Chem. Soc., 101, 6496 (1979).

(7) L.F. Schneemeyer, M.S. Wrighton, A. Stacy and M.J. Sienko, Appl. Phys. Lett., 36, 701 (1980).

(8) L.F. Schneemeyer and M.S. Wrighton, J. Am. Chem. Soc., (submitted).

(9) F.-R. F. Fan, H.S. White, B. Wheeler, and A.J. Bard, J. Am. Chem. Soc., (in press); J. Electrochem. Soc., 127, 518 (1980).

(10) H.J. Lewerenz, A. Heller, F.J. DiSalvo, J. Am. Chem. Soc., 102, 1877 (1980).

(11) W. Kautek, H. Gerischer, and H. Tributsch, Ber. Bunsenges. Phys. Chem., 83, 1000 (1979).

(12) N.E. Tokel-Takvoryan, R.E. Hemingway, and A.J. Bard, J. Am. Chem. Soc., 95, 6582 (1973).

(13) S.N. Frank, A.J. Bard, and A. Ledwith, J. Electrochem. Soc., 122, 898 (1975).

(14) S.M. Ahmed and H. Gerischer, Electrochima Acta, 24, 705 (1979).

(15) G. Nagasubramanian and A.J. Bard, following paper.

(16) A. R. Beal, W. Y. Liang, and H. P. Hughes, J. Phys., C9, 2449 (1976).

TABLE 1

Estimates of Flat-band Potentials and Donor Densities for n-WSe_2

Crystal	V_{fb}, V vs. SCE	n_D, cm^{-3}
WSe_2		
Type S	-0.22	1.3×10^{18}
	-0.36	2.0×10^{18}
	-0.42	1.8×10^{18}
Type E	-0.26	8.5×10^{18}
	-0.4 *	5.6×10^{19}

*Measured vs. Ag quasi-reference electrode and corrected to SCE with accuracy of $\sim \pm 0.1$ V.

TABLE 2

Voltammetric Data for Various Redox Couples at WSe_2

Couple	Pt[a]		Type S[b]		Type E[c]	
	V_{pa}	V_{pc}	V_{onset}	V_{pc}	V_{onset}	V_{pc}
I^-/I_2	0.35	0.1	0.00	----	-0.07	-0.08
Br^-/Br_2	0.69	0.25	0.05	-0.35	0.02	-0.12
Cl^-/Cl_2	1.09	0.82	0.55	----	0.21	-0.02
$Th^{0/+}$	1.26	1.20	0.60	0.76	0.67	0.75
$Ru(bpy)_3^{2/3+}$	1.33	1.27	0.91	0.96	----	----

Footnotes

(a) All values in V vs. SCE; E_{onset} = potential of photocurrent onset

(b) Under illumination; negligible dark anodic currents at Type S electrodes

(c) Under illumination; no well defined peaks in dark except for thianthrene oxidation, V_{pa} = 1.35 V; V_{pc} = 1.15 V

TABLE 3

Comparison of Current Densities at Type S and Type E

WSe_2 Electrodes in Solutions Containing Various Redox Couples

Redox Couple	Current[a], mA/cm^2			
	Type S		Type E	
	Dark[a]	Illuminated	Dark	Illuminated
I^-	< 0.1	0.66	< 0.1	0.71
Br^-	< 0.1	5.0	< 0.1	1.1
Cl^-	< 0.1	6.0	0.1	2.0
Th	< 0.1	3.2	2.4	2.4

(a) Dark current measured at potential of oxidation peak on Pt. Photocurrent measured at peak potential for Type E electrodes. Measured at current plateau for Type S electrode except for Br^- where i_{photo} was measured at 0.8 V.

TABLE 4

Characteristics of Several Photovoltaic Cells -

$n\text{-}WSe_2$ (Type S)/(MeCN), Cl^-, Cl_2/Pt[a]

Electrode[b]	Conc. TEACl	Fill Factor (max)	Power Efficiency	i_{sc} mA/cm^2	V_{oc} mV
A	sat'd	0.27	6.4	70	510
A	1.9 M	0.24	5.6	65	540
B	sat'd	0.26	10.4	125	480
C	sat'd	0.23	7.6	120	410
C	1.9 M	0.28	10.3	96	575
D	sat'd	0.20	7.3	90	544

(a) Irradiated with light > 590 nm. The power output of the lamp was 150 mW/cm^2.

(b) Electrodes A-D were different Type S crystals

SCHEME I

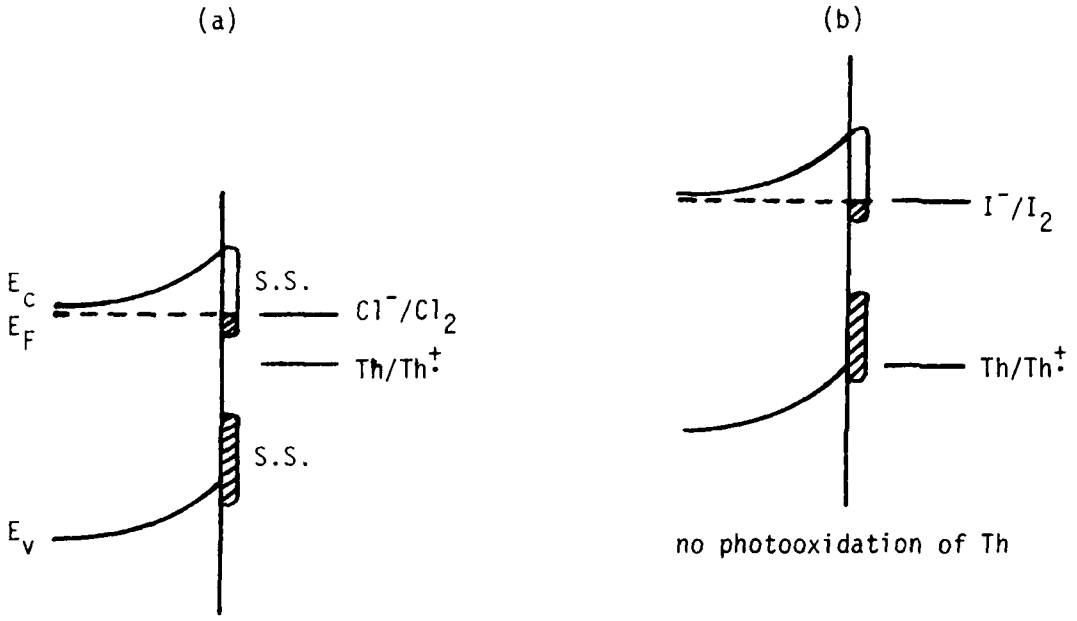

facile photooxidation of Th

no photooxidation of Th

E_c = conduction band edge

E_F = Fermi level

E_v = valence band edge

S.S. = surface state

FIGURE CAPTIONS

Fig. 1 Scanning electron micrographs of WSe_2 electrodes: (a) Type E; (b) Type S. Magnification X 100.

Fig. 2 Differential capacitance curve for Type E and Type S WSe_2 electrodes in MeCN containing 0.2 M TBAP. Scan rate, 5 mV/sec; applied AC voltage, 5 mV RMS. Frequency, 1000 Hz.

Fig. 3 Voltammetric behavior of Type S and Type E electrodes in MeCN - 0.2 M TBAP. Scan rate, 100 mV/sec, except for chopped light scans, 10 mV/sec.

Fig. 4 Mott-Schottky plots of (a) Type S and (b) Type E WSe_2 electrodes in MeCN - 0.2 M TBAP. (○) 200 Hz, (△) 500 Hz, (⊠) 1000 Hz.

Fig. 5 Voltammetric behavior of iodide in MeCN containing 0.2 M TBAP and TBAI. (a) Type S; $[I^-]$, 10 mM; (b) Type E; $[I^-]$, 15 mM. Scan rate, 100 mV/sec, except for chopped light scan at 10 mV/sec.

Fig. 6 Voltammetric behavior of bromide in MeCN containing 0.2 M TBAP and 10 mM Br^- (a) Type S; (b) Type E. Scan rate, 100 mV/sec except for chopped light scan at 10 mV/sec.

Fig. 7 Voltammetric behavior of chloride in MeCN containing 0.2 M TBAP and 10 mM Cl^- (a) Type S; (b) Type E. Scan rate, 100 mV/sec except for chopped light scan at 10 mV/sec.

Fig. 8 Voltammetric behavior of thianthrene in acetonitrile solution containing 0.2 M TBAP and 5 mM Th. (a) Type S; (b) Type E. Scan rate, 100 mV/sec except for chopped light scan at 10 mV/sec.

Fig. 9 Effect of bulk halide on dark currents at Type E n-WSe_2 electrode. (a) 5 mM thianthrene (Th); (b) 5 mM Th and 15 mM TBAI; (c) 5 mM Th and 10 mM TBABr; (d) 5 mM and 10 mM TMACl. Scan rate 100 mV/sec. 0.2 M TBAP as the supporting electrolyte.

Fig. 10 Effect of chloride on photooxidation of thianthrene; 5 mM Th, 10 mM TEACl and 0.2 M TBAP in acetonitrile solution. Solid lines indicate dark current; broken lines indicate photocurrent; same conditions of Th and Cl^- in mixed solution.

Fig. 11 Effect of dipping Type E n-WSe_2 electrode into 7 mM TEACl solution. (a) Dark oxidation of 5 mM Th on untreated electrode. (b) Photooxidation of 5 mM Th on untreated electrode. (c) Dark oxidation of Th after Cl^- treatment. (d) Photocurrent after Cl^- treatment.

Fig. 12 Performance characteristics of n-WSe_2/Cl^- (sat'd), Cl_2/Pt photoelectrochemical cells. 450 W Xe lamp fitted with a 590 nm cut-on filter used as light source. Power of focused light at electrode surface, 150 mW/cm^2.

Fig. 13 Effect of Cl^- and Cl_2 concentration on open-circuit photovoltage, V_{oc}, and short-circuit photocurrent, i_{sc}. Electrode area, 0.011 cm^2. Light source as in Fig. 12.

Fig. 14 Short-circuit photocurrent of WSe_2/Cl^- (1.9 M), Cl_2/Pt DEC cell as function of time. Electrode area, 0.015 cm^2.

Fig. 15 (a) Comparison of photopotentials developed at Type S (○) and Type E (△) WSe_2 electrode for several redox couples in MeCN. (b) Comparison of onset potential of photocurrent at Type S (○) and Type E (△) electrodes for several redox couples in MeCN.

SP472-3/A1

472:GAN:716:ddc
78u472-608

TECHNICAL REPORT DISTRIBUTION LIST, GEN

	No. Copies
Office of Naval Research Attn: Code 472 800 North Quincy Street Arlington, Virginia 22217	2
ONR Branch Office Attn: Dr. George Sandoz 536 S. Clark Street Chicago, Illinois 60605	1
~~ONR Area Office Attn: Scientific Dept. 715 Broadway New York, New York 10003~~	~~1~~
ONR Western Regional Office 1030 East Green Street Pasadena, California 91106	1
ONR Eastern/Central Regional Office Attn: Dr. L. H. Peebles Building 114, Section D 666 Summer Street Boston, Massachusetts 02210	1
Director, Naval Research Laboratory Attn: Code 6100 Washington, D.C. 20390	1
The Assistant Secretary of the Navy (RE&S) Department of the Navy Room 4E736, Pentagon Washington, D.C. 20350	1
Commander, Naval Air Systems Command Attn: Code 310C (H. Rosenwasser) Department of the Navy Washington, D.C. 20360	1
Defense Technical Information Center Building 5, Cameron Station Alexandria, Virginia 22314	12
Dr. Fred Saalfeld Chemistry Division, Code 6100 Naval Research Laboratory Washington, D.C. 20375	1
U.S. Army Research Office Attn: CRD-AA-IP P.O. Box 1211 Research Triangle Park, N.C. 27709	1
Naval Ocean Systems Center Attn: Mr. Joe McCartney San Diego, California 92152	1
Naval Weapons Center Attn: Dr. A. B. Amster, Chemistry Division China Lake, California 93555	1
Naval Civil Engineering Laboratory Attn: Dr. R. W. Drisko Port Hueneme, California 93401	1
Department of Physics & Chemistry Naval Postgraduate School Monterey, California 93940	1
Dr. A. L. Slafkosky Scientific Advisor Commandant of the Marine Corps (Code RD-1) Washington, D.C. 20380	1
Office of Naval Research Attn: Dr. Richard S. Miller 800 N. Quincy Street Arlington, Virginia 22217	1
Naval Ship Research and Development Center Attn: Dr. G. Bosmajian, Applied Chemistry Division Annapolis, Maryland 21401	1
Naval Ocean Systems Center Attn: Dr. S. Yamamoto, Marine Sciences Division San Diego, California 91232	1
Mr. John Boyle Materials Branch Naval Ship Engineering Center Philadelphia, Pennsylvania 19112	1

TECHNICAL REPORT DISTRIBUTION LIST, GEN

	No. Copies
Dr. Rudolph J. Marcus Office of Naval Research Scientific Liaison Group American Embassy APO San Francisco 96503	1
Mr. James Kelley DTNSRDC Code 2803 Annapolis, Maryland 21402	1

TECHNICAL REPORT DISTRIBUTION LIST, 359

	No. Copies
Dr. Paul Delahay Department of Chemistry New York University New York, New York 10003	1
Dr. E. Yeager Department of Chemistry Case Western Reserve University Cleveland, Ohio 41106	1
Dr. D. N. Bennion Department of Chemical Engineering Brigham Young University Provo, Utah 84602	1
Dr. R. A. Marcus Department of Chemistry California Institute of Technology Pasadena, California 91125	1
Dr. [illegible]. J. Auborn Bell Laboratories Murray Hill, New Jersey 07974	1
Dr. Adam Heller Bell Laboratories Murray Hill, New Jersey 07974	1
Dr. T. Katan Lockheed Missiles & Space Co, Inc. P.O. Box 504 Sunnyvale, California 94088	1
Dr. Joseph Singer, Code 302-1 NASA-Lewis 21000 Brookpark Road Cleveland, Ohio 44135	1
Dr. B. Brummer EIC Incorporated 55 Chapel Street Newton, Massachusetts 02158	1
Library P. R. Mallory and Company, Inc. Northwest Industrial Park Burlington, Massachusetts 01803	1
Dr. P. J. Hendra Department of Chemistry University of Southhampton Southhampton SO9 5NH United Kingdom	1
Dr. Sam Perone Department of Chemistry Purdue University West Lafayette, Indiana 47907	1
Dr. Royce W. Murray Department of Chemistry University of North Carolina Chapel Hill, North Carolina 27514	1
Naval Ocean Systems Center Attn: Technical Library San Diego, California 92152	1
Dr. C. E. Mueller The Electrochemistry Branch Materials Division, Research & Technology Department Naval Surface Weapons Center White Oak Laboratory Silver Spring, Maryland 20910	1
Dr. G. Goodman Globe-Union Incorporated 5757 North Green Bay Avenue Milwaukee, Wisconsin 53201	1
Dr. J. Boechler Electrochimica Corporation Attention: Technical Library 2485 Charleston Road Mountain View, California 94040	1
Dr. P. P. Schmidt Department of Chemistry Oakland University Rochester, Michigan 48063	1
Dr. H. Richtol Chemistry Department Rensselaer Polytechnic Institute Troy, New York 12181	1

TECHNICAL REPORT DISTRIBUTION LIST, 359

	No. Copies
Dr. A. B. Ellis Chemistry Department University of Wisconsin Madison, Wisconsin 53706	1
Dr. M. Wrighton Chemistry Department Massachusetts Institute of Technology Cambridge, Massachusetts 02139	1
Larry E. Plew Naval Weapons Support Center Code 30736, Building 2906 Crane, Indiana 47522	1
S. Ruby DOE (STOR) 600 E Street Washington, D.C. 20545	1
Dr. Aaron Wold Brown University Department of Chemistry Providence, Rhode Island 02192	1
Dr. R. C. Chudacek McGraw-Edison Company Edison Battery Division Post Office Box 28 Bloomfield, New Jersey 07003	1
Dr. A. J. Bard University of Texas Department of Chemistry Austin, Texas 78712	1
Dr. M. M. Nicholson Electronics Research Center Rockwell International 3370 Miraloma Avenue Anaheim, California	1
Dr. Donald W. Ernst Naval Surface Weapons Center Code R-33 White Oak Laboratory Silver Spring, Maryland 20910	1
Dr. R. P. Van Duyne Department of Chemistry Northwestern University Evanston, Illinois 60201	1
Dr. B. Stanley Pons Department of Chemistry University of Alberta Edmonton, Alberta CANADA T6G 2G2	1
Dr. Michael J. Weaver Department of Chemistry Michigan State University East Lansing, Michigan 48824	1
Dr. R. David Rauh EIC Corporation 55 Chapel Street Newton, Massachusetts 02158	1
Dr. J. David Margerum Research Laboratories Division Hughes Aircraft Company 3011 Malibu Canyon Road Malibu, California 90265	1
Dr. Martin Fleischmann Department of Chemistry University of Southampton Southampton 509 5NH England	1
Dr. Janet Osteryoung Department of Chemistry State University of New York at Buffalo Buffalo, New York 14214	1
Dr. R. A. Osteryoung Department of Chemistry State University of New York at Buffalo Buffalo, New York 14214	1
Mr. James R. Moden Naval Underwater Systems Center Code 3632 Newport, Rhode Island 02840	1

TECHNICAL REPORT DISTRIBUTION LIST, 359

	No. Copies
Dr. R. Nowak Naval Research Laboratory Code 6130 Washington, D.C. 20375	1
Dr. John F. Houlihan Shenango Valley Campus Pennsylvania State University Sharon, Pennsylvania 16146	1
Dr. M. G. Sceats Department of Chemistry University of Rochester Rochester, New York 14627	1
Dr. D. F. Shriver Department of Chemistry Northwestern University Evanston, Illinois 60201	1
Dr. D. H. Whitmore Department of Materials Science Northwestern University Evanston, Illinois 60201	1
Dr. Alan Bewick Department of Chemistry The University Southampton, S09 5NH England	1
Dr. A. Himy NAVSEA-5433 NC #4 2541 Jefferson Davis Highway Arlington, Virginia 20362	1
Dr. John Kincaid Department of the Navy Stategic Systems Project Office Room 901 Washington, DC 20376	1
M. L. Robertson Manager, Electrochemical Power Sonices Division Naval Weapons Support Center Crane, Indiana 47522	1
Dr. Elton Cairns Energy & Environment Division Lawrence Berkeley Laboratory University of California Berkeley, California 94720	1
Dr. Bernard Spielvogel U.S. Army Research Office P.O. Box 12211 Research Triangle Park, NC 27709	1
Dr. Denton Elliott Air Force Office of Scientific Research Bldg. 104 Bolling AFB Washington, DC 20332	1